JOURNAL OF GEOPHYSICAL RESEARCH, VOL. 101, NO. A9, PAGES 20,013–20,022, SEPTEMBER 1, 1996

Magnetosheath dynamics downstream of low Mach number shocks

M. E. McKean, N. Omidi,[1] and D. Krauss-Varban

Department of Electrical and Computer Engineering, University of California at San Diego
La Jolla

Abstract. The dissipation of the flow kinetic energy of solar wind ions at the quasi-perpendicular bow shock results in the formation of ion distributions that have large perpendicular temperature anisotropies. These anisotropies provide free energy for the growth of Alfvén ion cyclotron (A/IC) and mirror waves. The waves then make the ion distributions gyrotropic and substantially reduce their anisotropy. Although differences exist, many of the mechanisms governing wave generation and particle isotropization operate at both high and low Mach number shocks. These mechanisms are easier to study at low Mach number shocks because they proceed relatively slowly and the turbulence level is lower. Also, in general, the plasma beta is lower at the low Mach number bow shock, allowing for situations in which minority ion species like He^{++} can suppress proton cyclotron waves and thus play a larger role in sheath dynamics than they do at high Mach number shocks. For these reasons, we use two-dimensional hybrid simulations to model the heating of H^+ and He^{++} ions at the low Mach number bow shock and examine wave excitation and ion isotropization in the magnetosheath downstream. In agreement with observations and theory and in contrast to high Mach numbers, we find that the magnetosheath turbulence mostly consists of A/IC waves. Without helium ions, the A/IC wave activity is dominated by parallel propagating proton cyclotron waves. When helium ions are included at a low density, they tend to absorb these waves, leaving obliquely-propagating A/IC waves dominant, though at a lower intensity level. Proton heating at the shock is dominated by bulk perpendicular heating of the core, while the helium ions are heated only slightly. Instead, initially they gyrate around field lines downstream as a coherent, nongyrotropic bunch. Downstream, the protons are slowly isotropized through pitch-angle scattering by A/IC waves. The helium ions undergo perpendicular heating through absorption of proton waves and become more gyrotropic. The perpendicular heating drives the growth of helium cyclotron waves, which in turn reduce the anisotropy of the helium ions. Far downstream of the shock, obliquely-propagating helium cyclotron waves dominate the sheath turbulence.

1. Introduction

Ions incident on the Earth's magnetosphere carry a large bulk flow energy that must be dissipated at the bow shock. At quasi-perpendicular shocks, the primary mechanism for dissipation is through the heating of ions in the shock ramp, preferentially in the direction perpendicular to the ambient magnetic field. This heating process has two elements, the relative importance of which depends on the Mach number of the shock. For high Mach number shocks (those with a Mach number above the critical Mach number M_c), heating is dominated by reflected ions [*Sckopke et al.*, 1983]. These ions gain a large gyrovelocity relative to the bulk of the ions transmitted directly through the shock and thus contribute disproportionately to the heating. At low Mach number shocks, relatively few ions are reflected. For these shocks, the heating is dominated by the direct transmission of the bulk of the population [*Thomsen et al.*, 1985, *Sckopke et al.*, 1990].

At both high and low Mach number shocks, the shock-heated ion distributions have large perpendicular temperature anisotropies that make them linearly unstable to two electromagnetic ion instabilities. One of these is the Alfvén ion cyclotron (A/IC) instability, a transverse mode that generally has maximum growth along $\vec{B}_o$ (the background magnetic field) [*Kennel and Petschek*, 1966, *Davidson and Ogden*, 1975]. The other is the mirror instability, which is a com-

[1] Also at California Space Institute, University of California at San Diego, La Jolla.

Paper number 96JA01461.
0148-0227/96/96JA-01461$09.00

pressive mode that generally has maximum growth at highly oblique angles to $\vec{B}_o$ and has zero real frequency in the plasma rest frame [*Chandrasekhar et al.,* 1958, *Hasegawa,* 1975]. The A/IC and mirror instabilities then make the ion distributions gyrotropic and reduce their anisotropy. As the plasma flows away from the shock, it evolves to a quasi-steady state in which the ion distributions have a reduced anisotropy and the turbulence level is lower [*Sckopke et al.,* 1983, 1990].

The difference between low and high Mach number shocks is, of course, in the details. Conditions for wave excitation differ at subcritical and supercritical shocks because of amount of available free energy and the different shapes of the shock-heated ion distribution functions. Most of the free energy for wave growth at supercritical shocks is supplied by the reflected ions, which form a component of the ion distribution function that resembles a gyrophase-bunched ring beam [*Leroy and Winske,* 1983, *Sckopke et al.,* 1983]. At subcritical shocks, however, the free energy is supplied by the transmitted ions, which form an approximately bi-Maxwellian distribution function [*Thomsen et al.,* 1985, *Sckopke et al.,* 1990]. Also, the plasma beta is typically lower at the subcritical than at the supercritical bow shock, leading to different linear conditions for wave growth in each case. These differences in source populations, ion distribution functions, and plasma betas are reflected in the wave spectra in the magnetosheath. Downstream of high Mach number shocks, both mirror and A/IC waves are observed and are found at comparable energy levels. The sheaths of low Mach number shocks, however, are dominated by Alfvénic-like turbulence. The overall turbulence level is also much lower in the sheaths of low Mach shocks.

Most earlier work on the quasi-perpendicular bow shock and magnetosheath has concentrated on the high Mach number limit primarily it is more common than the low Mach bow shock. However, *Sckopke et al.* [1990] pointed out that the basic mechanisms operating downstream of high Mach number shocks are also at work downstream of low Mach shocks, except that the latter are easier to study in detail in the sheaths of low Mach shocks because the turbulence level is lower and the particle isotropization occurs more slowly. This is, of course, true not only for observed shocks but for simulated shocks as well. For example, in an earlier paper on the evolution of wave spectra and particle distributions downstream of high Mach shocks [*McKean et al.,* 1995a], we found that proton distributions had their anisotropy reduced so rapidly behind our simulated shock ramp that it proved challenging to investigate the details of the process. A major motivation for performing two-dimensional hybrid simulations of low Mach shocks is to closely scrutinize the excitation of waves and isotropization of particle distributions downstream of the shock.

Our earlier studies of the high Mach bow shock were motivated by observations suggesting that much wave activity in the quasi-perpendicular magnetosheath is generated at or near the shock and convected downstream. Observations by *Sckopke et al.* [1983, 1990] show that both compressive and transverse wave power peak near the shock and drop off quickly as the spacecraft move away from the shock. There is little direct evidence in sheath observations for *in situ* wave generation in the magnetosheath when the observing spacecraft is far removed from the magnetopause. We examined this idea by performing two-dimensional simulations of high Mach number quasi-perpendicular shocks and the associated magnetosheaths [*Omidi et al.,* 1994, *McKean et al.,* 1995a]. We found that both mirror and A/IC waves are indeed generated in and immediately downstream of the shock ramp and then convected further downstream. They are present at comparable intensities, with the intensities peaking near the shock and falling by an order of magnitude within several ion inertial lengths. We found no evidence that these waves are produced locally downstream. We confirmed that the free energy for the wave growth comes from the reflected ion population, which consists of 20% of the ions but has 60% of the energy. These ions have their free energy reduced rapidly in two overlapping but nonetheless distinct stages. In the first, the ions diffuse in gyrophase angle with little change in temperature anisotropy. Then wave activity pitch angle scatters the ions and reduces the temperature anisotropy. In a later paper [*McKean et al.,* 1995b], we included a low concentration of He^{++} ions in our high Mach number simulations. We found that they had little measureable impact on either the wave spectrum or proton dynamics. The helium ions themselves have their free energy reduced only over a much longer distance than the protons.

In this paper, we extend these earlier studies to low Mach number ($M_A = 2$), subcritical shocks. Our purpose is to examine how waves are generated at low Mach number shocks and to determine the evolutionary response of protons and helium ions to these waves. In particular, we want to measure the impact of He^{++} on the low Mach number magnetosheath. From theoretical considerations, we know that in low-β plasmas (which are characteristic of the low Mach number sheath), the presence of helium ions can help to suppress proton cyclotron waves [*Price et al.,* 1986, *Gary et al.,* 1993a, b]. If proton waves are suppressed, the possibility exists that the A/IC waves observed in the low Mach number magnetosheath [*Farris et al.,* 1993] are helium waves. The suppression of proton waves could in turn affect the evolution of proton distribution functions. Throughout we compare and contrast our results with our earlier high Mach ($M_A = 8$) number shock simulations and indicate what features of wave generation and ion isotropization are common to both low and high Mach shocks and what are not.

The impact of He^{++} ions is the subject of section 2. Then in section 3 we examine in detail data from a larger simulation that includes He^{++}. Both the nature of the wave spectra and the evolution of the proton and helium distributions are examined and compared to high Mach number results. We also examine the interplay between the H^+ and He^{++} ions and how that helps determine the wave spectra. Finally, in section 4 we summarize our results and present conclusions.

The two-dimensional hybrid code we use in this paper is similar to that used by *McKean et al.* [1995a] and uses a predictor-corrector method to solve for the fields [*Byers et al.*, 1978]. The simulation system is set in the $x - y$ plane, which is also the plane of the background magnetic field. In each simulation, particles incident on the right boundary are reflected while those incident on the left boundary are lost to the system. Periodic boundary conditions are used in the y direction. At the start of the run the simulation plasma consists of a flux of ions moving in the positive x direction (toward the right) and a comoving, neutralizing electron fluid. This ion flux is maintained by continuous injection of ions across the left boundary. A reflected ion beam forms when the incident beam reflects off the right boundary. A heated downstream state forms as a result of the interaction between these two beams, with a fast shock forming the transition between the incident (upstream) ion beam and the downstream plasma. The Alfvén Mach number M_A of the shock, the angle θ_{Bn} between the upstream magnetic field $\vec{B}_o$ and the shock normal (in the $-x$ direction), the upstream ion β_i and electron β_e, and the alpha particle density n_α are all input parameters and vary between simulations.

2. Impact of Helium Ions

To measure the impact of He^{++} ions, we ran two mid-size simulations that differ in the initial conditions only in the concentration of helium ions. For each simulation, $M_A = 2$, $\theta_{Bn} = 80°$, $\beta_i = 0.05$, and $\beta_e = 0.05$. The simulation system has a length $L_x = 100\ c/\omega_p$, where c is the speed of light and ω_p is the proton plasma frequency, and a width $L_y = 19\ c/\omega_p$. We use a grid spacing of $0.25\ c/\omega_p$ in both the x and y directions. We use a time step of $\delta t = 0.01\ \Omega_p^{-1}$, where Ω_p is the proton gyrofrequency. Our simulations were run for $50\ \Omega_p^{-1}$. One simulation has $n_\alpha = 0$, while the other has $n_\alpha = 0.04\ n_e$, where n_e is the electron density. This system has an anomalous resistive scale length of about $2\ c/\omega_p$ upstream of the shock and larger downstream. Thus the resistive scale length is well resolved by our grid spacing.

Unlike high Mach number simulations, we found that in the environment of a low beta, low Mach number shock, the presence of helium ions has an important impact on magnetosheath turbulence and a smaller impact on the proton population. How the presence of the helium ions affects the turbulence is illustrated in Figure 1. This figure shows the intensity as a function of x of compressive magnetic fluctuations (solid line), transverse fluctuations in the $x - y$ plane (thin dashed line), and transverse fluctuations in the z direction (thick dashed line). Figure 1a shows the results with $n_\alpha = 0$ and Figure 1b shows the results with $n_\alpha = 0.04\ n_e$. In both cases, transverse fluctuations are much more powerful than compressive fluctuations behind the shock front. This result agrees with observations downstream of subcritical shocks [*Sckopke et al.*, 1990, *Farris et al.*, 1993] and in stark contrast to both observations [*Sckopke et al.*, 1983, 1990] and simulations [*McKean et al.*, 1995a, b] of supercritical shocks. However, the profiles of transverse power are strikingly different. When no helium ions are present, oscillations in both transverse components of B rise in intensity rapidly at the shock and then remain at that power level further downstream. The intensities of the two components are approximately equal at some points, although in general the noncoplanar component (δB_z^2) is a factor of 2-3 times stronger. When $n_\alpha = 0.04\ n_e$, however, the intensity levels of both transverse components decline slowly away from the shock. The overall intensities are suppressed relative to the situation for $n_\alpha = 0$. Also, the power of noncoplanar oscillations is consistently about three times that of coplanar oscillations. By contrast, the intensity profile of compressive oscillations varies little between the two simulations except right at the shock itself, indicating that helium ions have little impact on the spectra of downstream compressive waves. Fourier analysis of these oscillations indicate that transverse oscillations are dominated by A/IC waves and compressive oscillations include both fast/magnetosonic waves (concentrated near the shock) and mirror waves. The lower level of transverse wave activity seen when helium ions are present is consistent with previous linear theory and homogeneous simulations that indicate that the presence of helium ions can suppress A/IC waves in low β plasmas [*Gary*, 1992, *Gary et al.*, 1993a, b].

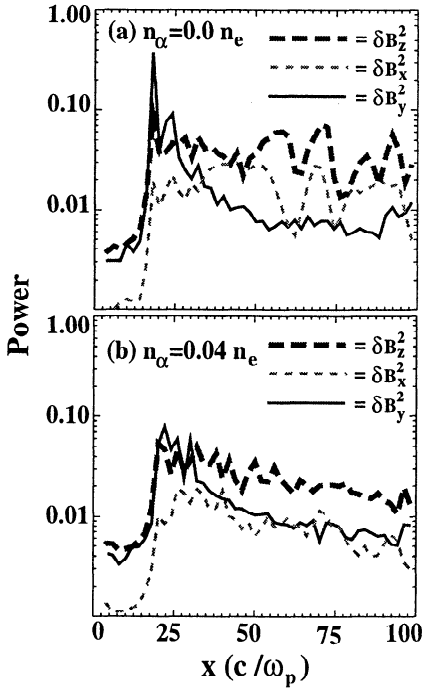

Figure 1. Profiles of power averaged over all y for compressive magnetic oscillations (B_y; solid lines), coplanar (with simulation plane) transverse oscillations (B_x; thin dashed lines), and noncoplanar oscillations (B_z; thick dashed lines). Shown are results for simulations with (a) $n_\alpha = 0$ and (b) $n_\alpha = 0.04\ n_e$.

Figure 2 illustrates how a low concentration of helium ions changes the turbulent wave spectra. Figure 2 shows the two-dimensional Fourier spectrum in k space

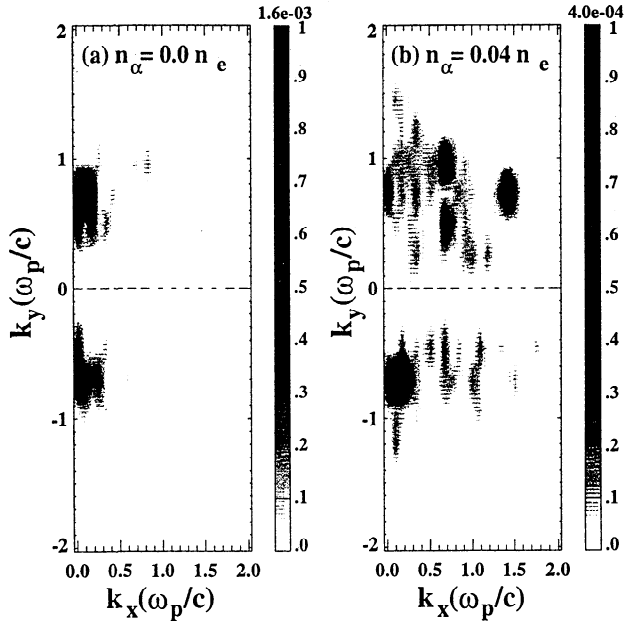

Figure 2. Spectral power in $k_x - k_y$ space for $x > 35\ c/\omega_p$. Results are shown for simulations with (a) $n_\alpha = 0$ and (b) $n_\alpha = 0.04\ n_e$.

of magnetic fluctuations in the z direction in a region downstream ($x > 35\ c/\omega_p$) of the shock front. Figure 2a shows the results for the case with $n_\alpha = 0$; Figure 2b shows the results for $n_\alpha = 0.04\ n_e$. When no helium ions are present, the spectrum is dominated by waves propagating nearly parallel and antiparallel to $\vec{B}_o$, which is approximately parallel to the y axis. These waves are left-handed circularly polarized, which is characteristic of A/IC waves. For $n_\alpha = 0.04\ n_e$, the parallel and antiparallel propagating modes are both suppressed (note that the scale maximum for Figure 2b is only one quarter that for Figure 2a). Overall, obliquely propagating waves contribute more power to the total than parallel-propagating modes. These oblique modes are mostly linearly polarized. Given that for A/IC waves the perturbations are mostly perpendicular to the plane of the wave vector and the background magnetic field, this would help explain why, in Figure 1b, the intensity of noncoplanar transverse oscillations is so much higher than the intensity of coplanar oscillations. The relative intensities of the two transverse components appears to be consistent with observations of *Farris et al.* [1993] (compare Figure 5 of that paper), although the authors indicate that θ_{Bk} for these waves is typically less that 10°, which is less consistent with our results.

The simplest explanation for the difference between the spectra and intensity profiles in the two simulations is that the helium ions are strongly resonant with parallel propagating A/IC waves emitted by the protons and absorb them. Given the continuing decline of transverse wave power with x (Figure 1b), the absorption apparently occurs throughout the downstream region rather than being just a local effect (i.e., confined to some narrow region). The helium ions also have a small, although noticeable, impact upon the proton dynamics. The downstream temperature anisotropy of the protons is slightly higher (2.9) when the helium ions are present than when they are not (2.5). Because the intensity of A/IC waves is much lower, the actual efficiency with which A/IC waves reduce proton anisotropy is greater when helium ions are present. This result is in accord with earlier theoretical and simulation results [*Gary et al.*, 1993c]. Whether the oblique modes shown in Figure 2b exist in both simulations and are simply obscured in the $n_\alpha = 0$ simulation or whether some oblique modes are generated only in the $n_\alpha = 0.04\ n_e$ simulation is one of the topics addressed in the next section.

3. Main Simulation Results

For the simulation whose results we discuss in this section, we increased the system length to $L_x = 150\ c/\omega_p$ and width to $L_y = 50\ c/\omega_p$, slightly increased the plasma betas ($\beta_i = 0.1$ and $\beta_e = 0.1$), and doubled the size of the grid spacing in the y-direction to $0.5\ c/\omega_p$. Other parameters remained the same. Our simulation was run for $110\ \Omega_p^{-1}$.

Figure 3 shows profiles of the densities of H^+ and He^{++} in units of their upstream values (Figure 3a), the temperature anisotropies of the two ion species (Figure 3b), v_x in the simulation frame for both species (Figure 3c), $T_\perp$ and $T_\parallel$ for He^{++} ions (Figure 3d), the same for protons (Figure 3e), and the magnitude

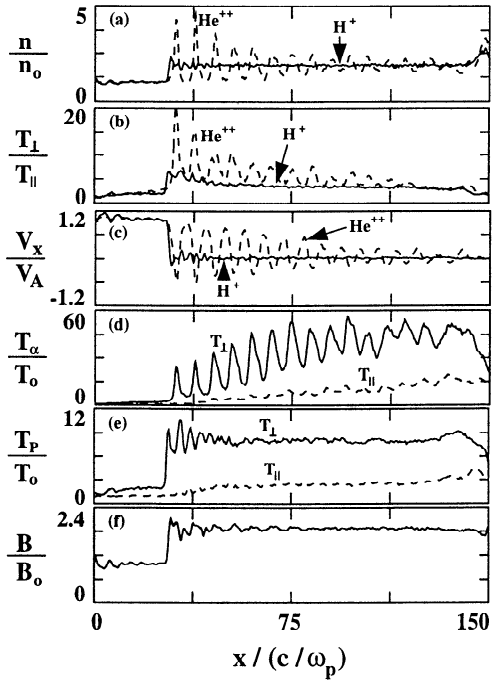

Figure 3. Profiles of plasma parameters for simulation discussed in section 3. All parameters are averaged over y. Shown are (a) densities of H^+ (solid line) and He^{++} (dashed line); (b) temperature anisotropies of the two ion species; (c) v_x (shock normal velocity) of both ion species; (d) perpendicular temperature $T_\perp$ and parallel temperature $T_\parallel$ of helium ions; (e) $T_\perp$ and $T_\parallel$ of protons; and (f) magnetic field magnitude.

of the magnetic field B (Figure 3f). All quantities are averaged over y. The behavior of plasma parameters is similar to that found in our high Mach number simulations, except that changes associated with the shock happen more slowly, that is, over longer scale lengths. The magnetic field magnitude reaches an average of 2.1 B_o in the shock overshoot before settling to its downstream value of 1.8 B_o. The proton density also slightly overshoots its downstream values before settling down to about 1.8 n_{p0}, where n_{p0} is the upstream proton density. The perpendicular temperature peaks at about 10 T_o in the shock ramp, while the parallel temperature shows almost no change. Instead, $T_{\|}$ climbs slowly after the shock crossing, while $T_\perp$ drops slightly. The anisotropy average is about 6 at the shock and decreases only slowly downstream. If we define the quantity $\delta A_p = A_p - A_{pmin}$, where A_p is the proton anisotropy $T_\perp/T_{\|}$ and A_{pmin} is its minimum downstream value (about 2.9 in the present simulation). If we use A_{pmin} as an estimate of the asymptotic value of A_p, then the e-folding scale length for the decrease in δA_p is approximately 20 c/ω_p. This compares with approximately 5 c/ω_p for shocks with $M_A = 8$ in our earlier simulations [*McKean et al.*, 1995a, b], consistent with a slower evolution of proton distributions at low Mach shocks. The minimum sheath anisotropy of 2.9 is much higher than seen downstream of high Mach number shocks (approximately 1.2). The higher value is a consequence of the higher anisotropy threshold for the A/IC instability when the plasma beta is low, as it is in our simulations [*Gary et al.*, 1993b].

In contrast with proton parameters, helium ion parameters show a great deal of variation not only near the shock but throughout the downstream region. This variation is due to the fact that the He^{++} ions are strongly nongyrotropic after passing through the shock. As will be discussed later, the helium ions gyrate around magnetic field lines as a cohesive bunch and only lose that cohesiveness over several tens of c/ω_p. Unlike the proton $T_\perp$, which only shows an increase at the shock, the helium $T_\perp$ on average increases from the shock to $x \simeq 100\ c/\omega_p$. The helium $T_{\|}$ shows increases throughout the simulation box. In the downstream region, the helium anisotropy is on average higher than the proton anisotropy (about 4.5 compared to 2.9), although the minimum anisotropy is only slightly higher. The reasons for the different behavior of these helium parameters is explored in detail later in this section.

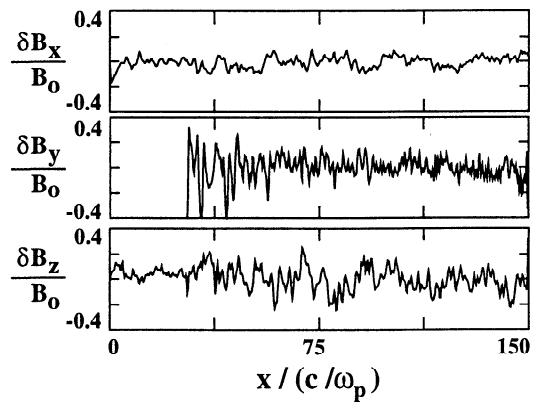

Figure 4. Oscillations about average downstream field at $y = 50\ c/\omega_p$ in (a) B_x, (b) B_y, and (c) B_z.

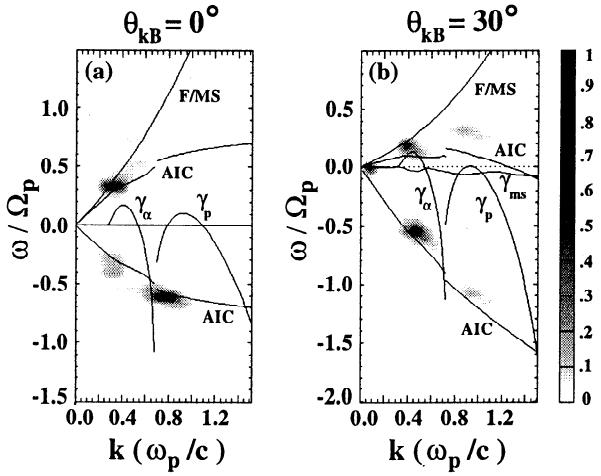

Figure 5. Power spectra of fluctuations in B_z for propagation angles of (a) $\theta_{kB} = 0°$ and (b) $\theta_{kB} = 30°$. Also shown are dispersion curves for the fast/magnetosonic (F/MS) mode and forward and backward propagating Alfvén ion cyclotron (A/IC) mode, including curves showing the growth/damping rates for the F/MS mode (γ_{ms}), and the proton (γ_p) and helium (γ_α) branches of the A/IC mode.

The characteristics of magnetic perturbations downstream are illustrated in Figure 4, which shows profiles of δB_x, δB_y, and δB_z as a function of x for a single value of y at the end of the run. The scales show the deviation from the average downstream values of these variables. Figure 4 demonstrates that the results shown in Figure 1b for a smaller simulation box hold for this simulation as well. Fluctuations in B_y (essentially compressive) dominate the wave activity right at the shock and for about 20 c/ω_p downstream of the shock. Then they decay rapidly in amplitude. Noncoplanar transverse fluctuations (δB_z) start growing at the shock and peak in amplitude about 20 c/ω_p downstream. These fluctuations dominate the wave activity after $x \simeq 60\ c/\omega_p$ and decay slowly in amplitude above $x \simeq 75\ c/\omega_p$. Fluctuations in B_x show behavior similar to those in B_z but are only about as intense as the downstream B_y fluctuations.

To identify the dominant wave modes downstream of the shock, we performed Fourier analyses of B_z fluctuations in the region between $x = 60\ c/\omega_p$ and $x = 140\ c/\omega_p$ downstream of the shock front and compared them with results of linear theory calculations based upon bi-Maxwellian ion (H^+ and He^{++}) distributions and a homogeneous system. Both the Fourier analyses and linear theory were performed in the shock rest frame. The integration for the Fourier transforms was performed between $\Omega_p t = 60$ and $\Omega_p t = 110$. The results of these calculations are displayed in Figure 5. Figure 5a shows the $\omega - k$ diagram for modes propagating parallel to the ambient magnetic field. Figure 5b shows

the same for a propagation angle of 30°. In each panel, the dispersion curves for the forward-propagating (in the direction of $\vec{B}_o$) fast/magnetosonic mode and the forward and backward propagating A/IC modes are indicated. The breaks in the dispersion curves for the A/IC modes are due to the existence of separate cyclotron modes for the protons and helium ions at low β. The growth rates (multiplied by a factor of 10) for the proton and helium modes are also shown.

As can be seen in Figure 5, for both oblique and parallel propagation the modes that dominate the power spectra lie on or close to the dispersion curves for Alfvénic modes. Although some fast/magnetosonic waves also appear to be present, they contribute little to the wave activity. In particular, the local spectral peak for $\theta_{kB} = 0°$ at $\omega \simeq 0.3\ \Omega_p$ and $k \simeq 0.35\ c/\omega_p$ has a polarization consistent with A/IC waves, although it lies adjacent to dispersion curves for both the A/IC and F/MS modes. More interesting are the source ion populations of the observed waves. At parallel propagation, both proton and helium Alfvénic modes are present and strong, with the single most intense mode being a proton mode. At oblique propagation, on the other hand, helium modes are much more intense than proton modes. The growth rate for the helium mode also changes little between the two angles, while the proton mode growth rate drops off to zero at $\theta_{kB} = 30°$. Since the total power of oblique Alfvénic modes is comparable to the power in parallel modes downstream of the shock (see Figure 2b), these results suggest that helium ions, despite their low concentration, may be a greater source of A/IC wave activity in the low Mach magnetosheath than proton ions.

To understand why this may be the case, we now examine the evolution of particle distribution functions downstream of the shock. We begin by examining the evolution of the proton distribution function, shown in Figure 6. The distribution functions depicted represent an integration in real space at the end of the run over all y and over 1 c/ω_p in x. The left column shows two-dimensional cuts through proton distributions in the $v_{\|} - v_z$ plane, while the right column shows cuts through proton distributions perpendicular to the magnetic field ($v_x - v_z$ space). The first row shows the approximately isotropic distribution upstream of the shock. The second row shows the heating of the protons in the shock ramp. The heating is essentially only in the direction perpendicular to the magnetic field ($v_x - v_z$ plane). This is achieved mainly through bulk heating of the transmitted ions, although a small (about 1%) initially reflected component with a large perpendicular velocity is also apparent. The reflected ions can be seen in the left panel at $x = 31\ c/\omega_p$ as a high-energy tail with $v_z \gtrsim 1.5\ v_A$. The transmitted ions remain gyrotropic as they pass through the shock, whereas the small reflected component does not (note the small nongyrotropic component at high positive v_x and v_z at $x = 31\ c/\omega_p$). The proton distribution evolves slowly as the protons move away from the shock. The nongyrotropy of the reflected component disappears first, and the reflected ions merge with the transmitted ions to form an approximately bi-

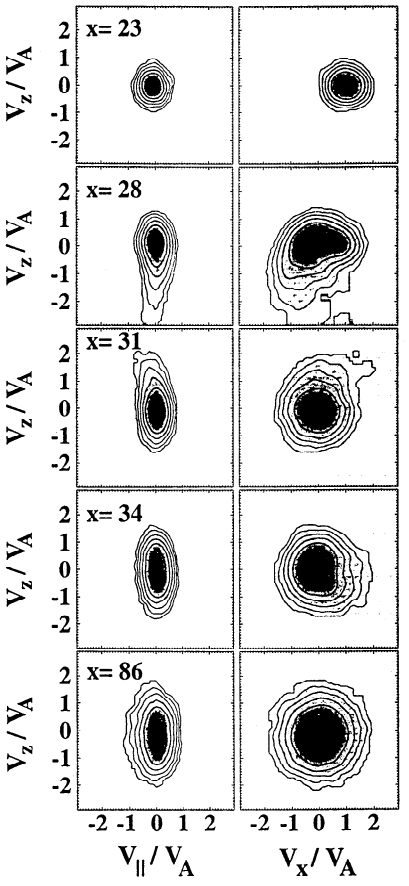

Figure 6. Two-dimensional cuts through the proton distribution function at the indicated locations. (left) The distribution in the $v_{\|} - v_z$ plane, where v_z is the component of perpendicular velocity out of the simulation plane. (right) The distribution in the $v_x - v_z$ plane, essentially the plane perpendicular to the average magnetic field. Each distribution is averaged over all y and 1 c/ω_p in x. The shock is located at $x = 28\ c/\omega_p$.

Maxwellian distribution (third and fourth rows). By 60 c/ω_p downstream of the shock ramp (bottom row), the protons have been substantially heated in the parallel direction as a result of pitch-angle scattering by A/IC waves. The evolution depicted in Figure 6 is qualitatively similar to the evolution of proton distributions observed by *Sckopke et al.* [1990] downstream of the low Mach number bow shock.

Figures 7 and 8 depict the evolution of the helium ion distribution function. Figure 7 show the perpendicular velocity ($v_x - v_z$) phase space of helium ions just downstream of the shock, and Figure 8 shows $v_{\|} - v_z$ and $v_x - v_z$ phase space in the same format as Figure 6, though at different locations in the second to fourth rows. The helium ions undergo almost no heating in the shock ramp proper. Instead, they are deflected by the stronger magnetic field in the ramp and downstream of it, and begin gyrating around downstream field lines in bulk. This gyration occurs because, in the downstream (simulation) frame, there is essentially no $E \times B$ drift velocity because the motional electric field vanishes. Protons, whose dynamics basically determine the shock structure, are decelerated at the shock front, but

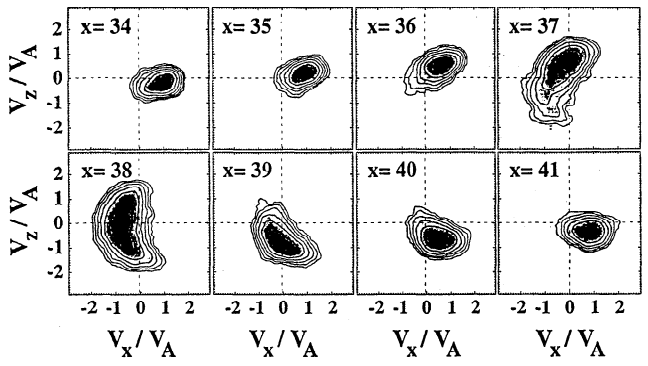

Figure 7. Two-dimensional cuts through the helium distribution function in the plane perpendicular to average $\vec{B}$ in the region just downstream of the shock.

alpha particles, as a consequence of their larger mass-to-charge ratio, are only slightly slowed down. Thus the upstream drift velocity is added ito the alpha particles' gyrovelocity vectors downstream of the shock. Since the magnitude of the drift velocity is generally much larger than the magnitude of the particles' gyrovelocities, the helium ions initially appear in $v_x - v_z$ phase space as a cohesive bunch gyrating around the origin (Figure 7). Because of this, one can in effect assign a gyrophase angle to a measured distribution function. By comparing Figure 7 with Figure 3, one can see that the measured density, temperatures, and temperature anisotropy of the bulk He^{++} are strong functions of this angle. As a result of this dependence, the overall evolution of the helium ion distribution can be followed most effectively by comparing distribution functions with approximately the same gyrophase angle.

This is the motivation for the choice of locations in Figure 8. From the second row down, the measured distributions have approximately the same gyrophase angle as the distribution at $x = 34\ c/\omega_p$. They are set apart by approximately the distance the downstream plasma moves away from the shock in two He^{++} gyroperiods. As can be seen by comparing the first row (upstream helium distribution) with the second row, helium ions are heated preferentially in the direction perpendicular to the background magnetic field immediately behind the shock. The perpendicular heating continues through $x = 86\ c/\omega_p$ (bottom row), but because $T_{||}$ also increases, the anisotropy slowly declines (compare the local minima of the helium anisotropy in Figure 3). There are two basic reasons for the perpendicular heating. One reason is the conversion of gyration kinetic energy into thermal energy. Through the interaction of the sheath waves with He^{++} ions, the strong nongyrotropy of the helium distribution is reduced and the net gyration speed of the helium population decreases. The ions are heated in the process. Notice that the center of the He^{++} distribution in $v_x - v_z$ space moves from $\sim 1.0\ v_A$ at $x = 34\ c/\omega_p$ to $\sim 0.2\ v_A$ at $x = 86\ c/\omega_p$. At the latter location, the distribution is nearly gyrotropic. The second cause of perpendicular heating is absorption by the helium ions of waves emitted by the protons. This topic is discussed in detail

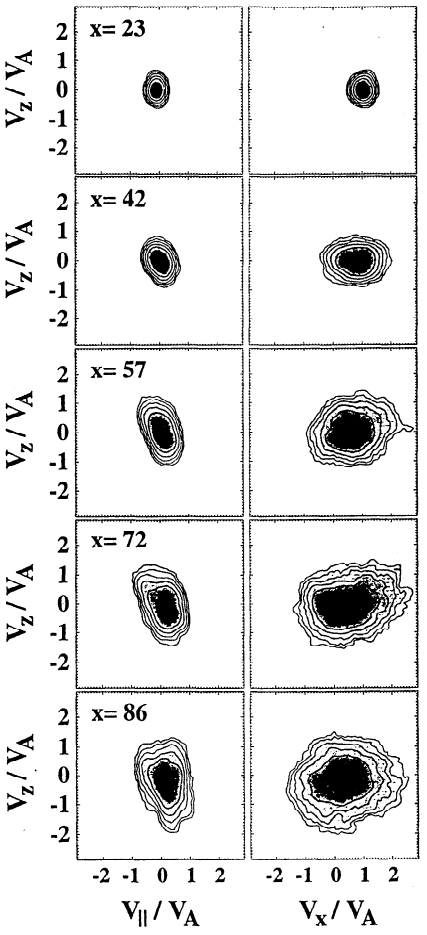

Figure 8. Two-dimensional cuts through the proton distribution function at the indicated locations. The figure is formatted in the same way as Figure 6.

below. The source of parallel heating is essentially the same as for protons, that is, pitch angle scattering by A/IC waves.

Figure 9 compares one-dimensional cuts (solid curves) of downstream $f(v_\perp)$ for both protons and helium ions for the simulation discussed in this section (Figure 9a) and the high Mach number shock (Figure 9b) described by *McKean et al.* [1995b]. The selected $f(v_\perp)$ is integrated over all of y and 17 c/ω_p in x far downstream of the shock. In the same manner as *Fuselier and Schmidt* [1995], we attempt to fit ring-beam distributions (dashed curves) of the form

$$f(v_{\perp s}) = n_s \exp[(v_{\perp s} - v_{0s})^2 / 2v_{Ts}^2]$$

to our "observed" distributions. In this equation, v_{0s} is the gyrovelocity of the center of the distribution function of species s and v_{Ts} is the thermal velocity. For the low Mach number shock, $v_{0p} = 0$, $v_{Tp} = 1.9\ v_A$, $v_{0\alpha} = 0.5\ v_A$, and $v_{T\alpha} = 2.4\ v_A$. For the high Mach number shock, $v_{0p} = 0$, $v_{Tp} = 0.56\ v_A$, $v_{0\alpha} = 0.3\ v_A$, and $v_{T\alpha} = 0.53\ v_A$. For the low Mach number shock, the fitted distribution functions fit the proton and helium data well. There is little indication of a halo consisting of initially reflected ions [cf. *Fuselier and Schmidt*, 1995]. For the high Mach shock, the pro-

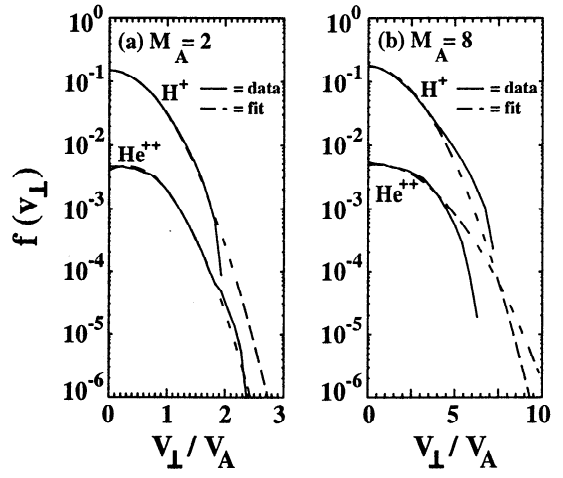

Figure 9. Distribution of $v_\perp$ for H^+ and He^{++} ions far downstream of (a) a simulated $M_A = 2$ shock and (b) a simulated $M_A = 8$ shock. The actual data are shown by solid curves. Fits to the data using one-dimensional drifting Maxwellian distribution functions are shown by dashed curves.

ton distribution shows evidence of such a halo (above $v_\perp = 4\ v_A$). The helium distribution, on the other hand, shows no such halo. The disagreement at higher energies between the data and the fitted distribution function for He^{++} ions is probably a consequence of low statistics. These results are qualitatively similar to those of *Fuselier and Schmidt* [1995]. Note, however, that the limited number of particles in our simulations prevents us from having the same dynamic range of particle energies as *Fuselier and Schmidt* [1995].

Although one-dimensional cuts of the helium ion distribution show a ring-beam form, it is important to note that a true ring-beam never develops. Instead, in $v_x - v_z$ space the helium ion distribution retains its original shape as a cohesive, nongyrotropic bunch until the perpendicular thermal velocity, which increases with x, exceeds the gyration velocity, which decreases. Once this happens, the two-dimensional distribution resembles a hot, gyrotropic Maxwellian centered (approximately) on the origin. However, it never resembles a ring. This result differs from the results of *Motschmann and Glassmeier* [1993], who used one-dimensional simulations to probe the heating of heavy ions in the magnetosheath. They used O^{6+} ions and found that they formed ring-beam-like distributions downstream of the shock. This is possibly a consequence of their one-dimensional geometry, which excludes the excitation of parallel-propagating A/IC waves such as those that interact with the helium ions in our simulation. Our result also suggests that the helium distributions observed by *Fuselier and Schmidt* [1995] were not true ring beams.

We now turn to a discussion of the interaction between protons and helium ions, and the effects of this interaction on the wave spectra. Figure 10a shows profiles of the energy densities of the H^+ (solid line) and He^{++} (dashed line) ion populations. The energy densities include both flow energy and thermal energy, and are computed in the shock rest frame. Each point represents an average over all y and over 6.25 c/ω_p in x. At the shock ramp, the proton population loses about 12% of its energy due to wave excitation. The helium population also loses a few percent of its energy, but this loss is swamped by the proton loss and consequently, most of the wave energy found near the shock ramp derives from the protons. Further downstream, however, the situation is more complicated. The helium energy density shows a net gain (about 20% at $x = 140\ c/\omega_p$), while the proton energy density stays at about the same level. This result indicates that wave absorption, most likely of proton cyclotron waves, is a factor in the heating of the helium ions.

The absorption of proton cyclotron waves by helium ions can probably explain the relative depletion of parallel propagating waves in this simulation compared to low Mach simulations with no helium ions (cf. Figure 2). It cannot readily explain the dominance of helium modes far downstream of the shock (cf. Figure 5) because relatively little energy is given up by the helium ions at the shock. The excitation and growth of helium modes is explored in Figure 10b. This panel shows the power as a function of x for two A/IC wave modes with $\theta_{kB} = 30°$. One mode is a proton cyclotron mode with $k \simeq 0.9\ \omega_p/c$ (solid line), and the other mode is a helium cyclotron mode with $k \simeq 0.4\ \omega_p/c$ (dashed line). These are the two dominant modes shown in Figure 5b. The modes were isolated using a combination of wavelet and Fourier filtering techniques [cf. *Muret and Omidi,*

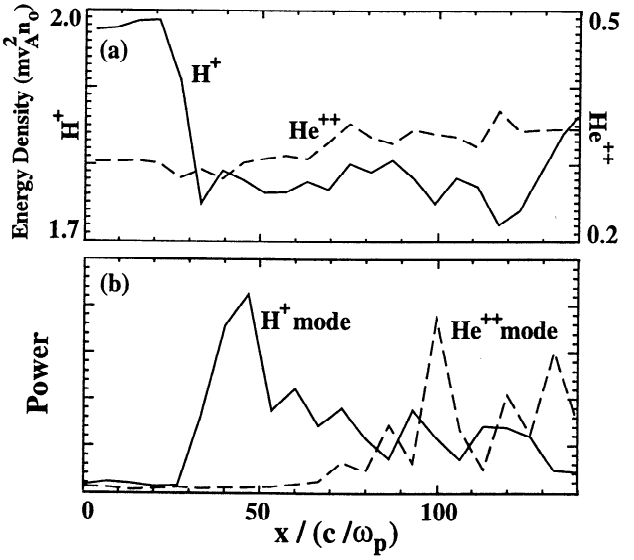

Figure 10. Profiles of different quantities from low and high Mach number simulations. (a) Energy density for H^+ ions (solid line) and He^{++} ions (dashed line). The proton energy density has been offset by 1.5 $mv_A^2 n_o$ so that it can be compared directly to the helium ions. (b) Powers of the dominant H^+ and He^{++} modes shown in Figure 5b. (c) Powers of a short wavelength A/IC mode ($k \simeq 0.05\ c/\omega_p$) and a long wavelength A/IC mode ($k \simeq 0.2\ c/\omega_p$) from a simulation of a quasi-perpendicular shock with $M_A = 8$.

1995]. The proton mode is excited at the shock ramp and peaks in power at about $x = 50\ c/\omega_p$. Its power then declines until it reaches a steady level at about $x = 85\ c/\omega_p$. The helium mode, on the other hand, shows no noticeable growth until $x \simeq 70\ c/\omega_p$. Further downstream, it is on average more intense than the proton mode. Comparing the growth of the helium mode with the profile of helium energy density, one can see that the helium energy actually increases when the helium wave mode is increasing in power, that is, when helium ions are absorbing proton waves. Indeed, this absorption may drive the growth of helium cyclotron waves. Absorption of proton waves raises the helium perpendicular energy, increasing the helium anisotropy. This increases the free energy available for the growth of helium cyclotron waves. The helium waves in turn pitch angle scatter the helium ions, increasing their parallel temperature and reducing their anisotropy. This local, downstream generation of helium waves constitutes an exception to our general result, in this paper and *McKean et al.* [1995a, b], that waves observed downstream of quasi-perpendicular shocks are generated at the shock and just convected downstream.

4. Summary and Conclusions

In this paper, we used two-dimensional hybrid simulations to model the low Mach number quasi-perpendicular bow shock and magnetosheath with the goal of understanding the mechanisms for wave generation and ion isotropization downstream. In agreement with observations and theory, we found that the low Mach magnetosheath turbulence is dominated by A/IC waves. By comparing the results of two simulations that had identical initial conditions except that one had a tenuous helium component while the other did not, we found that the presence of helium ions reduced the intensity level of A/IC waves. In particular, we found that helium ions primarily absorbed parallel-propagating Alfvén waves, thereby enhancing the relative contribution of both obliquely propagating A/IC waves and compressive waves (including mirror waves). This is compatible with previous linear theory for low β plasmas and results of periodic simulations of the same. Far downstream of the shock, these oblique modes actually have greater power than parallel-propagating modes. Further analysis of the results of a third, larger simulation showed that the oblique A/IC wave activity is itself dominated by helium modes. These helium cyclotron waves mostly grow far from the shock. Their growth appears to be driven in part by the absorption of proton cyclotron waves by helium ions, which drives up their perpendicular energy and hence the source of free energy for cyclotron emission. The growth of helium cyclotron waves in the downstream region constitutes an exception to our more general conclusion regarding waves observed in the quasi-perpendicular magnetosheath: That these waves are generated at the shock (both high and low Mach numbers) and are convected downstream.

In terms of particle heating at the shock and subsequent isotropization, we found that most proton heating comes from perpendicular heating of the core transmitted component. Around 1% of protons are reflected once before entering the downstream region, but they are less important energetically. Downstream of the shock, wave-particle interactions rapidly remove the nongyrotropy of the reflected ions. The proton anisotropy of the total distribution is reduced more slowly through pitch angle scattering by proton cyclotron waves. This is consistent with observations downstream of low Mach shocks [*Sckopke et al.*, 1990]. Upon passage through the shock, He^{++} ions gyrate around field lines as a cohesive bunch in velocity phase space. Interaction with and absorption of proton cyclotron waves reduces the bulk gyrating motion and heats the helium ions in the direction perpendicular to the magnetic field. In turn, the growth of helium cyclotron waves pitch angle scatter the helium ions, reducing the helium anisotropy.

Because some of the mechanisms for wave generation and particle isotropization are the same at high and low Mach number shocks, we have also considered the relevance of these results to the high Mach number bow shock. In the case of the reduction of proton free energy, we have found in this study that the reflected ions are gyrotropized before the entire distribution is isotropized. We had found this to be the case in our high Mach simulations [*McKean et al.*, 1995a], but, in general, proton free energy is lost so quickly that the details are difficult to discern. For the low Mach number shock, we found that the reflected protons are difficult to distinguish from the main population far downstream. In contrast, for high Mach number shocks, a high-energy halo that consists of reflected ions is apparent (Figure 9). This difference is due to the small number of reflected ions at the low Mach shock. In the case of the reduction of helium free energy, the same progression of gyrotropization followed by isotropization was found downstream of both low and high Mach shocks [*McKean et al.*, 1995b]. The details of this process, though, as outlined above is much clearer at low Mach number shocks. Because of the different character of the wave activity at high Mach number shocks, it is not clear that helium ions downstream of these shocks lose their free energy through the same mechanisms operating at low Mach number shocks.

Whether the mechanisms at work for wave generation and particle isotropization we have found in our simulation results operate in the magnetosheath of the actual low Mach number, quasi-perpendicular bow shock is a question that can be answered by future theoretical and observational studies. This study is limited by the fact that only two-dimensional studies have been used, the planar geometry, and the assumption that upstream of the shock, the protons and helium ions have the same velocity. In fact, at the Mach number treated in this paper, the protons and helium ions have a significant differential velocity upstream of the shock when the solar wind speed is large ($\gtrsim 500$ km/s), with the helium ions about an Alfvén speed faster [*Marsch et al.*, 1982a, b]. A problem with modeling this velocity differential

in our simulations (which we have attempted) is that this velocity difference leads to a beam instability in the upstream region that rapidly destabilizes the simulation system and causes the program to crash. Partial results from these test runs suggest that the helium ions disperse somewhat more quickly in gyrophase space when the velocity differential exists but that the basic dynamics of helium gyrotropization and isotropization remain about the same. This is a question that needs additional investigation.

Observationally, the Cluster mission may give us an opportunity to see whether or not the mechanisms examined in this paper operate in the Earth's magnetosheath. For example, the magnetic field data from the four spacecraft used in this mission should allow us to identify the characteristic frequencies, wavelengths, propagation directions, and polarizations of the turbulence in the low Mach number sheath. This could allow observers to clearly identify whether the A/IC waves observed there are proton or helium waves, and if both are present, their relative intensities. Data on the evolution of the helium distribution function will allow us to see if there is evidence for the complex mechanism for helium isotropization that we have uncovered in this study.

Acknowledgments. This research was supported by the NASA Space Physics Theory Program grant NAG5-1492 and the NASA Supporting Research and Technology Program grant NAGW-3975. N. Omidi's work was performed under the auspices of the California Space Institute. Computations for this work were carried out on the CRAY C90 at the San Diego Supercomputing Center, which is operated by the National Science Foundation. We also thank P. Muret for his work in developing the diagnostic tools used here and H. Karimabadi for useful discussions.

The Editor thanks D. W. Swift and J. Giacalone for their assistance in evaluating this paper.

References

Byers, J. A., B. I. Cohen, W. C. Condit, and J. D. Hansen, Hybrid simulations of quasi-neutral phenomena in magnetized plasmas, *J. Comput. Phys., 27,* 363, 1978.

Chandrasekhar, S., A. N. Kaufman, and K. M. Watson, The stability of the pinch, *Proc. R. Soc. London A, 245,* 435, 1958.

Davidson, R. C., and J. M. Ogden, Electromagnetic ion cyclotron instability driven by ion energy anisotropy in high-beta plasmas, *Phys. Fluids, 18,* 1045, 1975.

Farris, M. H., C. T. Russell, and M. F. Thomsen, Magnetic structure of the low beta, quasi-perpendicular shock, *J. Geophys. Res., 98,* 15,285–15,294, 1993.

Fuselier, S. A., and W. K. H. Schmidt, H^+ and He^{2+} heating at the Earth's bow shock, *J. Geophys. Res., 99,* 11,539–11,546, 1995.

Gary, S. P., The mirror and ion cyclotron anisotropy instabilities, *J. Geophys. Res., 97,* 8519–8529, 1992.

Gary, S. P., B. J. Anderson, R. E. Denton, S. A. Fuselier, M. E. McKean, and D. Winske, Ion anisotropies in the magnetosheath, *Geophys. Res. Lett., 20,* 1767, 1993a.

Gary, S. P., S. A. Fuselier, and B. J. Anderson, Ion anisotropy instabilities in the magnetosheath, *J. Geophys. Res., 98,* 1481–1488, 1993b.

Gary, S. P., M. E. McKean, and D. Winske, Ion cyclotron anisotropy instabilities in the magnetosheath, *J. Geophys. Res., 98,* 3963–3971, 1993c.

Hasegawa, A., *Plasma Instabilities and Nonlinear Effects,* Springer-Verlag, New York, 1975.

Kennel, C. F., and H. E. Petschek, Limit on stably trapped particle fluxes, *J. Geophys. Res., 71,* 1–28, 1966.

Leroy, M. M., and D. Winske, Backstreaming ions from oblique Earth bow shocks, *Ann. Geophys., 1,* 527–536, 1983.

Marsch, E., K.-H. Mühlhäuser, H. Rosenbauer, R. Schwenn, and E. M. Neubauer, Solar wind and helium ions: Observations of the Helios solar probes between 0.3 and 1 AU, *J. Geophys. Res., 87,* 35–51, 1982a.

Marsch, E., K.-H. Mühlhäuser, R. Schwenn, H. Rosenbauer, W. Pilipp, and E. M. Neubauer, Solar wind protons: Three-dimensional velocity distributions and derived plasma parameters between 0.3 and 1 AU, *J. Geophys. Res., 87,* 52–72, 1982b.

McKean, M. E., N. Omidi, and D. Krauss-Varban, Wave and ion evolution downstream of quasi-perpendicular bow shocks, *J. Geophys. Res., 100,* 3427–3437, 1995a.

McKean, M. E., N. Omidi, D. Krauss-Varban, and H. Karimabadi, Wave and particle evolution downstream of quasi-perpendicular shocks, *Adv. Space Res., 15,* 319–322, 1995b.

Motschmann, U., and K.-H. Glassmeier, Simulations of heavy ion ring and shell distributions downstream of the bow shock, *Geophys. Res. Lett., 20,* 987–990, 1993.

Muret, P., and N. Omidi, Analysis of steepened magnetosonic waves using wavelet transforms and neural networks, *J. Geophys. Res., 100,* 23,465–23,479, 1995.

Omidi, N., A. O'Farrell, and D. Krauss-Varban, Sources of magnetosheath waves and turbulence, *Adv. Space Res., 14,* 45–54, 1994.

Price, C. P., D. W. Swift, and L.-C. Lee, Numerical simulation of nonoscillatory mirror waves at the Earth's magnetosheath, *J. Geophys. Res., 91,* 101–112, 1986.

Sckopke, N., G. Paschmann, S. J. Bame, J. T. Gosling, and C. T. Russell, Evolution of ion distributions across the nearly perpendicular bow shock: Specularly and nonspecularly reflected gyrating ions, *J. Geophys. Res., 88,* 6121–6136, 1983.

Sckopke, N., G. Paschmann, A. L. Brinca, C. W. Carlson, and H. Lühr, Ion thermalization in quasi-perpendicular shocks involving reflected ions, *J. Geophys. Res., 95,* 6337–6352, 1990.

Thomsen, M. F., J. T. Gosling, S. J. Bame, and M. M. Mellott, Ion and electron heating at collisionless shocks near the critical Mach number, *J. Geophys. Res., 90,* 137–148, 1985.

D. Krauss-Varban, M. E. McKean, and N. Omidi, Department of Electrical and Computer Engineering, University of California, San Diego, La Jolla, CA 92093-0407. (email: mmckean@ece.ucsd.edu)

(Received October 18, 1995; revised May 2, 1996; accepted May 7, 1996.)